Edited by
Petra Fromme

WILEY-BLACKWELL

Photosynthetic Protein Complexes

A Structural Approach

With book website

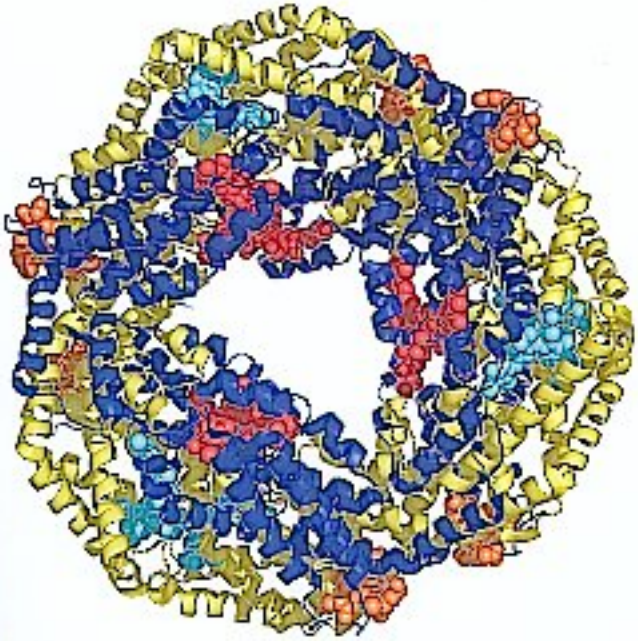

9
The Structure of the H^+-ATP Synthase from Chloroplasts

Bettina Böttcher and Peter Gräber

9.1
Introduction

Proton translocating ATPases (H^+-ATP synthase, F-type ATPase, F_0F_1, EC 3.6.1.34) occur in the cytoplasmic membranes of bacteria (e.g. *E.coli*, EF_0F_1), in the thylakoid membranes of chloroplasts (CF_0F_1), and in the inner mitochondrial membranes (MF_0F_1). The protein complexes of the electron transport chains are also located in these energy converting membranes. During photosynthesis and respiration, the electron transport is coupled with a transmembrane proton transport that leads to the generation of a transmembrane eletrochemical potential difference of protons, $\Delta\tilde{\mu}_{H^+}$. The H^+-ATP synthases couple the $\Delta\tilde{\mu}_{H^+}$-driven backflux of protons across the membrane with the synthesis of ATP from ADP and inorganic phosphate [1]. Hydrolysis of ATP provides the free energy for almost all energy requiring processes in cells; therefore, H^+-ATP synthases are central enzymes of energy metabolism in cells. For example, the mitochondrial H^+-ATP synthases in humans produce between (50–70) kg ATP per day.

H^+-ATP synthases from different sources have a similar bipartite overall structure. A hydrophilic F_1-part extrudes from the membrane into the aqueous phase. It contains the nucleotide and phosphate binding sites and catalyzes the hydrolysis/synthesis of the β-γ-phosphate bond in ATP. A hydrophobic F_0-part is integrated into the membrane. It contains the proton binding sites and catalyzes the proton transport through the membrane. The F_1- and F_0-part are connected by a central and a peripheral stalk to which subunits from both parts contribute (Figure 9.1).

H^+-ATP synthases are multi-protein complexes. Although they are similar in shape, their subunit composition depends on the source of the enzyme. The H^+-ATP synthase from *Escherichia coli*, EF_0F_1 is the simplest enzyme, with eight different subunits. The most complex one is the enzyme from mitochondria, MF_0F_1, with at least 13 different subunits. The H^+-ATP synthase from chloroplasts, CF_0F_1, has nine different subunits (see Table 9.1 for subunit compositions of CF_0F_1, EF_0F_1, and MF_0F_1). CF_1 consists of five different subunits which are

Photosynthetic Protein Complexes: A Structural Approach. Edited by P. Fromme
Copyright © 2008 WILEY-VCH Verlag GmbH & Co. KGaA, Weinheim
ISBN: 978-3-527-31730-1

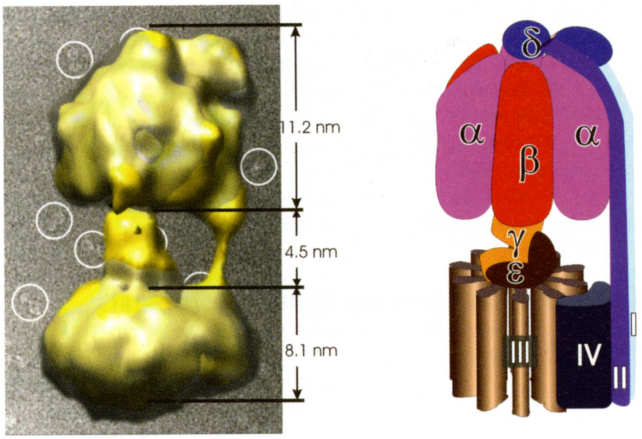

Figure 9.1 Left: Background electron micrograph of CF_0F_1 in vitrified buffer. Some enzymes are marked with white circles. Image analysis was carried out with 10000 particles and a three-dimensional map was calculated. A surface representation of this map is shown is shown in the foreground. Right: Cartoon of the subunit organization in CF_0F_1. Subunits designated with Greek letters form F_1, subunits labeled with Roman numbers form F_0.

designated by Greek letters (α, β, γ, δ, ε) [58]. They have the stoichiometry $\alpha_3\beta_3\gamma\delta\varepsilon$ [59, 60]. The four subunits of CF_0 are numbered by Roman numerals (I, II, III, IV) [61, 62] and have the subunit stoichiometry I II III_{14} IV [53, 56]. The nomenclature of the subunits in the different organisms is inconsistent. This is especially true for the F_0 subunits. Subunit IV is the largest subunit of CF_0 and is homologous to subunit a in *E. coli*. Subunits I and II form the second stalk and have homologies to subunit b from *E. coli*. Subunit III_{14} forms the rotor of the H^+-ATP synthase and corresponds to the c-ring in *E. coli*. In Table 9.1 homologous subunits are collected in the same rows.

The enzyme mechanism of H^+-ATP synthases from different sources is similar. According to the binding change mechanism [64, 66], the three catalytic nucleotide binding sites, located mainly on the β-subunits, adopt three different conformations. Each conformation allows a specific catalytic step: substrate binding, formation, and splitting of the β-γ–phosphate bond and product release. The three different conformations are caused by different interactions of each β-subunit with the γ-subunit. Rotation of the γ-subunit changes simultaneously its interaction with all three β-subunits. This gives rise to a strong cooperativity of the three catalytic sites. The high resolution structure of F_1 from mitochondria [71] shows directly that the γ-subunit interacts differently with the three β-subunits (see 9.2).

The mechanism of coupling of proton translocation and rotation is described by the following model [67, 68]: Subunits III form a ring in the membrane (see 9.3). They can be protonated from the internal aqueous phase through an entrance channel formed by subunits III and IV. The uncharged protonated amino acid

Table 9.1 Stoichiometry of subunits and structural data of F-type H^+ATPases and their subcomplexes.

E. coli		Chloroplasts		Mitochondria	
Subunits (Stoichiometry)	**Structural data Method, pdb-id, reference**	**Subunits (Stoichiometry)**	**Structural data Method, reference**	**Subunits (Stoichiometry)**	**Structural data Method, reference**
α (3)	–	α (3)	–	α (3)	–
β (3)	–	β (3)	–	β (3)	–
γ (1)	–	γ (1)	–	γ (1)	–
δ (1)	NMR N-term-domain **1ABV, 2A7U** [2, 3]	δ (1)	–	OSCP (1)	NMR, 1BO5 [4]
ε (1)	NMR, 1BSH,1BSN [5, 6] X-ray, 1AQT[7]	ε (1)	–	δ (1)	–
–		–	–	ε (1)	–
–		–	–	IF1 (1)	X-ray, 1GMJ [8]
EF_1	EM [9–12]	CF_1	EM [13–15]	MF_1	EM [16–18]
a (1)	NMR, **1C17** [19]	IV (1)	–	a (1)	–
b (2)	NMR **1B9U** [20] **1L2P** [21]	I (1)	–	b (1)	–
		II (1)	–		
c (11)	NMR, 1C0V; 1A91[22] 1C99[19]	III (14)	–	c (10)	–
–	–	–	–	d (1)	–
–	–	–	–	F_6 (1)	NMR, 1VZS [23]
–	–	–	–	e (1)	–
–	–	–	–	f (1)	–
–	–	–	–	g (1)	–
EF_0	AFM [24–26]	CF_0	–	MF_0	–
EF_0F_1	EM [27–29]	CF_0F_1	AFM[30], EM [31–36]	MF_0F_1	EM [35, 37–40]
Sub-complexes					
–	–	$(\alpha\beta)_3$	X-ray 1FX0 [41] 1KMH [42]	–	–
$(\alpha\beta)_3\gamma\varepsilon$	X-ray, 1D8S [43]	–	–	$(\alpha\beta)_3\gamma\delta\varepsilon$	X-ray 2HLD [44] 1E79 [45]
$\gamma\varepsilon$	X-ray 1FS0 [46] 1JNV [47]	–	–	–	–
–	–	–	–	$((\alpha\beta)_3\gamma IF1)_2$	X-ray, 1QHH [48] EM [49]
				$(\alpha\beta)_3\gamma\delta\varepsilon c_{10}$	X-ray, 1QO1 [50]
c11(tartaricus)	X-ray **1YCE** [51] AFM/EM [52]	III_{14}	AFM [53, 54] EM [55]	–	
ac_{12}	NMR/ modelling **1C17** [19]	$IV\ (III)_{14}$	AFM [56]	–	
–	–	–	–	bdF_6	X-ray 2CLY [57]

Homologous subunits of the different enzymes are given in the same rows.
Subunit stoichiometries of the F_0-parts are estimated.
IF_1 is the inhibitor protein of MF_0F_1.
EM: electron microscopy; NMR: nuclear magnetic resonance; X-ray: X-ray diffraction.
Structures used for modelling of CF_0F_1 in Figures 9.2– 9.4 are shown bold.

IIIglu61 can move from the hydrophilic entrance channel into the hydrophobic membrane interior. This movement of the ring shifts simultaneously a protonated IIIglu61 into an asymmetrically located, hydrophilic channel with an exit to the outer aqueous phase where the proton is released. This mechanism explains the generation of a rotational movement by proton translocation through the membrane and the transmembrane Δ pH determines the direction of rotation. Since the III-ring interacts non-covalently with γ and ε, these subunits rotate together with the III-ring. During proton transport coupled ATP hydrolysis the direction of rotation is opposite to that during ATP synthesis as shown with single molecule spectroscopy [75, 76]. In the F_1 part chemical energy is used to generate rotational movement of the γ subunit, in the F_0 part osmotic energy is used to generate rotational movement of the III-ring. In the holoenzyme both parts are connected and form a chemiosmotic machine. Since the magnitude of the enzyme is in the nm-range, it is called a "nanomotor."

In this review, collected structural data for H^+-ATP synthases and their subunits (see Table 9.1 for overview) are presented to generate a pseudo atomic model of CF_0F_1. Most of the direct structural knowledge on CF_0F_1 comes from electron microscopy (EM), atomic force microscopy (AFM), and the crystallization and structure resolution with x-ray crystallography. The only available atomic model of a CF_0F_1-subcomplex represents the $\alpha_3\beta_3$-complex [41, 42]. In order to overcome this lack of high-resolution structural information, homology models for most of the subunits (γ,δ,ε, I, II, III, IV) were generated with MODELLER [69] using known structures of orthologous subunits as references (Table 9.1, bold). For the modeling, the sequences of target and reference were aligned according to the PFAM data-base [70]. The 3D-map of CF_0F_1 (Figure 9.1 left, [32]) derived from electron microscopy served as a scaffold for integrating the diverse structural information into a pseudo-atomic model of CF_0F_1.

9.2 The Structure of CF_1

The hydrophilic CF_1-part can be separated from the membrane integrated CF_0-part. First insights into the structure of CF_1 came from electron microscopy and image analysis of negatively stained particles that show a pseudo hexagonal arrangement of $\alpha_3\beta_3$ with $\gamma\delta\varepsilon$ located asymmetrically in the centre [13, 14]. These projection maps still lacked three-dimensional information. Only later localization of subunit δ of the *E. coli* ATP synthase by immuno electron microscopy revealed its location at the top, outside of the $\alpha_3\beta_3$-complex [65]; whereas, γ and ε form the central stalk that is anchored inside the $\alpha_3\beta_3$-hexagon by two long helices of γ [45, 71]. In the pseudo-hexagonal view of $\alpha_3\beta_3$, the centers of mass of the α-subunits extend further from the two central helices of γ than those of the β-subunits, which also enables distinguishing between α and β subunits in low-resolution maps.

The three $\alpha\beta$-pairs in $\alpha_3\beta_3\gamma$ can adopt different conformations. In the mitochondrial complex, the orientation of the central stalk relative to the $\alpha\beta$-pairs deter-

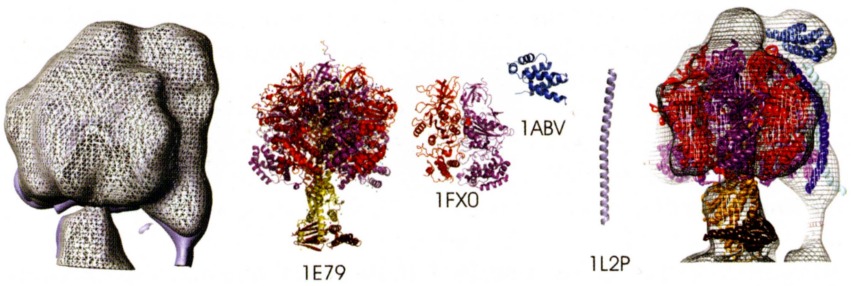

Figure 9.2 Superposition of the CF_1-part of the three dimensional map of CF_0F_1 derived from electron microscopy (grey) with models of the subunits. The α-subunits are shown in magenta, β in red, γ in yellow, ε in brown, δ in light blue, I and II in dark blue. The homology models of γ and ε are calculated from the $\alpha_3\beta_3$ γ δ template (center, 1E79, mitochondrial δ is homologous to chloroplast ε). The αβ-pairs are derived from the chloroplast $\alpha_3\beta_3$(center, 1FXO). The homology model of the N-terminal region of δ was based on the structure of δ from *E. coli* (center, 1ABV), the models of subunit I and II are both based on the structure of the dimerization region of the b-subunits from *E. coli* (center, 1L2P).

mines the conformational state of the catalytic nucleotide binding sites. These sites are located on the β-subunits at the interface to the adjacent α subunits. In the mitochondrial $\alpha_3\beta_3\gamma\delta\varepsilon$-complex, one of the catalytic binding sites is empty (E), one has an ADP (D) loosely bound, and the third has a tightly bound non-hydrolysable ATP analogue(AMPPNP) (T).

This is different in the $\alpha_3\beta_3\gamma\varepsilon$ complex of chloroplasts [41, 42], where the crystallographic threefold axis superimposes with the pseudo-sixfold axis of the complex, making the αβ-pairs indistinguishable and the electron density for γ and ε uninterpretable. However, the αβ pair is well resolved and shows a similar conformation as the αβ-pair of the mitochondrial complex in the D or T conformation, but is incompatible with an αβ-pair in the E state. The significance of this difference to the mitochondrial enzyme is still unclear.

In order to obtain a pseudo-atomic model for CF_1, the structure of the mitochondrial $(\alpha\beta)_3\gamma\delta\varepsilon$ (1E79, [45]) was used as a template (Figure 9.2 center). The three copies of the αβ-pairs of CF_1 (1FX0, [41], Figure 9.2 centre) and the modeled γ and ε subunits were matched to the template. The newly generated sub-complex was placed into the upper half of the 3D-map of CF_0F_1 (Figure 9.2, right). The model accounted for most of the density in CF_1, except for a region at the top of $\alpha_3\beta_3$ and at the periphery of one of the α-subunits. Into the region at the top, the modeled N-terminal domain of the δ-subunit was placed adjacent to an α-subunit as determined by NMR-spectroscopy. This left room for the C-terminal domain of δ at the central top of $\alpha_3\beta_3$, in agreement with the localization by immuno-electron microscopy in EF_0F_1 [65]. Models of the dimerization region of subunits I and II were fitted into the unaccounted density at the periphery of the α-subunit to which δ is bound. The positioning of subunits I and II in close proximity to the α-subunit is in agreement with cross-linking data between the α- and the b-subunits in *E.*

coli [72]. Figure 9.2, right, shows a superposition of the 3D-map derived from electron cryo-microscopy (grey) with $\alpha_3\beta_3$ from chloroplasts and the homology models of γ, ε, δ and I + II (in color).

9.3 The Structure of CF_0

CF_0 consists of four different subunits, I, II, III, and IV. Subunit IV (homology to *E. coli a*) was initially missed by SDS-PAGE as a component of CF_0 [62] because it stains only weakly by Coomassie Blue. Later, subunit IV was identified in silver stained gels as a genuine component of CF_0F_1 [61].

Subunit III (homology to *E. coli c*) exists in multiple copies and is the major component of CF_0. It forms a stable complex that remains intact even during SDS gel electrophoresis and requires heating in SDS-buffer for dissociation into monomers [55]. The subunit-III complex has an oblate shape with a membrane spanning length of 6.1 nm and a diameter of 6.2 nm and a stoichiometry of III_{12} [55] was suggested. Later, investigations of the subunit III-complex with atomic force microscopy (AFM) allowed the identification of the individual subunits in the complex resulting in 14 monomers per complex [53]. The stoichiometry of the subunits in the ring seems to be fixed by the shape of the subunits and the contacts to their nearest neighbors as revealed by incomplete complexes that maintain their diameter [54]. Comparison of AFM images of CF_0, $III_{14}IV$ and III_{14} show an additional density inside the III-ring in sub-complexes that contain subunit IV [56]. This lead to the assumption that subunit IV is located in the centre of the III-ring. However, this notion is in contradiction to the current structural and functional understanding of CF_0. An alternative explanation for the presence of the additional density is the variable amounts of lipids that plug the ring similarly as observed for the c-ring of *I. tartaricus* [73].

For modeling the III_{14}-ring, the c-ring of *I. tartaricus* (1YCE, [51]) was used as a template (Figure 9.3 top, centre). This ring consists of only 11 subunits. Each subunit is a helical hairpin. The N-terminal helices form an unusually tightly packed inner ring. The C-terminal helices fill the grooves between the N-terminal helices and form an outer ring. Sodium ions bind between C-terminal and N-terminal helices in the center of the membrane, where the diameter of the ring is smallest. Since *I. tartaricus* is a sodium-translocating ATP synthase, it is likely that these sodium ions identify the potential proton-binding sites in H^+-ATP synthases.

With 11 subunits, the c-ring of *I. tartaricus* is significantly smaller in diameter than the III_{14}-ring in chloroplasts. For modeling of the III-ring, the inter-subunit packing of the homology models of subunit III was kept similar as in *I. tartaricus*, but the stoichiometry of subunits and the diameter of the ring were adjusted according to the AFM data ([53, 74], Figure 9.3 top, left). The modeled ring matched the surface topology measured by AFM (Figure 9.3 top, right).

Currently, no experimental data on the structure of subunit IV (subunit a) is available. For placing the subunit IV relative to the III-ring, the model of the *E.*

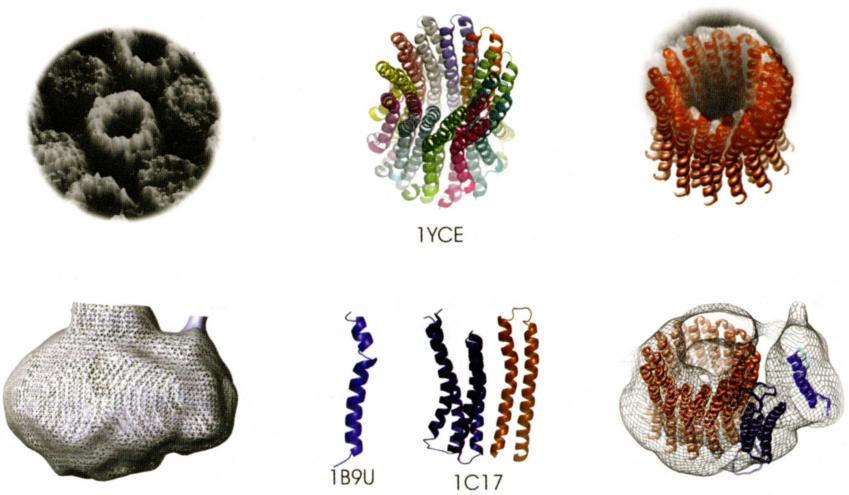

Figure 9.3 Top: Superposition of the structure of the subunit III_{14}-complex from atomic force microscopy (grey, left) with the homology model of subunit III_{14} (light brown, right), based on the structure of III_{14}-complex from *Ilyobacter tartaricus* (center, 1YCE). Bottom: Superposition of the CF_0-part of the three-dimensional map of CF_0F_1 from electron microscopy (grey) with homology models. The subunit III_{14}–complex is shown in light brown. The N-terminal domains of subunit I and II are based on the structure of this region of the b-subunit from *E. coli* (1A9U, centre), blue. The model of subunit IV is based on the structure of the a-subunit from *E. coli* (1C17, centre) blue.

coli ac_{12}-complex served as a template, based on computational structure prediction (1C17, [19], Figure 9.3, bottom, centre). The resulting $III_{14}IV$-model was placed as a whole into the CF_0-part of the 3D-map of CF_0F_1 (Figure 9.3 bottom, left). The CF_0-part in the 3D-map is considerably larger than the modeled $III_{14}IV$, which makes the placement tentative. The reason for the discrepancy in size is the presence of a detergent micelle that shields the hydrophobic regions of CF_0, which are usually integrated into the thylakoid membranes. The outline of the III-ring can be recognized in the 3D-map inside the detergent micelle. The III-ring protrudes at the bottom from the detergent micelle (Figure 9.3 bottom, left) and is closed by an unidentified density, which is similar to the lipids that plug the c-ring of *I. tartaricus* [73]. Adjacent to the III-ring, underneath the peripheral stalk, a free volume is detected that is not accounted for by the detergent micelle (Figure 9.3 bottom, right). The free volume is a region with electron density in the 3D-map from electron cryo microscopy, in which no protein is found after placing the homology model. This volume is separated from the III-ring by a gap, which is much wider than the distance between the III-ring and subunit IV in the model. Therefore, the $III_{14}IV$ model was placed with subunit IV adjacent to the gap. The membrane parts of subunits I and II were modeled according to the N-terminal region of the *E. coli* subunit b ([20], Figure 9.3, bottom, centre) and were positioned into the free volume directly underneath the peripheral stalk (Figure 9.3, bottom right).

9.4
The Structure of CF_0F_1

The homology model of CF_0F_1 (Figure 9.4 center) is obtained by placing the models of CF_1 and CF_0 (Figures 9.2 and 9.3) into the 3D-map of CF_0F_1 (Figure 9.4, left). Despite the wealth of structural information on orthologous subunits, some domains and fragments of subunits could not be modeled. These are the C-terminal region of the δ-subunit (Figure 9.4, green columns at the top of F_1), two helices of subunit IV (Figure 9.4, green columns in front of the rotor), and the region between the membrane integrated parts of subunits I and II and the CF_1 attached regions of subunits I and II (Figure 9.4, green columns in the peripheral stalk). According to EPR-measurements of Spin-Spin interactions after spin-labeling of subunits b in the stalk region, the b-subunits in EF_0F_1 are spaced by 2.9 nm in this region [63], which is far more than expected for a coiled coil structure. Therefore, the two green columns, representing the missing helical regions of I and II, were placed well apart, but inside, the scaffold provided by the image reconstruction (Figure 9.4, right).

The superposition of the pseudo atomic model of CF_0F_1 with the EM map shows that the model accounts for all density except the detergent micelle that surrounds the region that is usually membrane integrated, and the plug that closes the III-ring from the lumenal side. Thus, the combination of the low resolution electron microscopy data with the homology models of subunits and subunit complexes gives a structural model of CF_0F_1 with a higher resolution

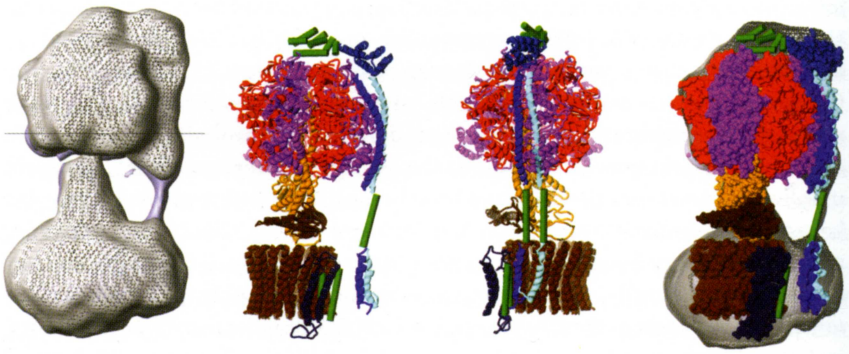

Figure 9.4 Left: Three-dimensional map of CF_0F_1 (grey). The line indicates the slice which is represented in Figure 9.5. Center: The homology models shown in Figures 9.2 and 9.3 are combined to a pseudo-atomic model of CF_0F_1. Regions which could not be modeled are filled with green columns. These are the C-terminal domain of subunit δ, the tether domain of subunits I and II between CF_0 and CF_1 and two helices of subunit IV. The pseudo-atomic model of CF_0F_1 is shown in two different side views, rotated by 90°. The rotation axis is perpendicular the membrane (color code as in Figures 9.2 and 9.3). Right: Superposition of the 3D-map from electron microscopy with the pseudo atomic model of CF_0F_1. Unaccounted density in CF_0 can be mainly attributed to the detergent micelle and a plug at the lumenal side of the III-ring.

which will be useful in designing future experiments on structure function relations.

9.5 Structure and Function of CF_0F_1

H^+-ATP synthases have three catalytic nucleotide binding sites on the β-subunits and three non-catalytic nucleotide binding sites on the α-subunits; they use a remarkable mechanism to synthesize, or to hydrolyze, ATP ("binding change mechanism" [64, 66]). According to this mechanism, the catalytic sites work cooperatively. At a given time, each site has a different conformation. For example, site 1 is in an open conformation and can bind substrates; site 2 is in a closed conformation, it does not exchange substrates with the aqueous phase and there is equilibrium between bound products (ATP) and bound substrates (ADP and phosphate) at this site. Site 3 is partly open and contains loosely bound products. These different conformations of the biochemically identical β-subunits are generated by the different interactions with the γ-subunit located asymmetrically in the centre of the $\alpha_3\beta_3$-complex. If the γ-subunit rotates in the F_1-part, the interactions with all three β-subunits change and, therefore, the conformations of all catalytic sites change simultaneously. At each catalytic site the sequence of the three conformation leads to the synthesis of one ATP per site, when the γ-subunit rotates by 360°.

The coupling between proton transport and chemical rotation is effected as follows [67, 68]. The deprotonated amino acid Glu61 of subunit III is located in a hydrophilic access channel, provided by subunit IV, in the middle of the membrane. Protonation of this amino acid via subunit IV drives the rotation of the III_{14} ring thereby moving the protonated (uncharged) subunit III from the access channel into the hydrophobic membrane core. Since subunit III forms a ring, the neighbouring unprotonated subunit III simultaneously moves into the access channel and can be protonated in the following step. Deprotonation occurs when the protonated subunit III has moved so far that it reaches the second hydrophilic channel in subunit IV, which has an exit to the other side of the membrane. Protons are released to the aqueous phase on the other side of the membrane. Since subunit III is in contact with subunits γ and ε, this leads to a rotation of the γ ε III_{14}-complex (rotor) relative to the $\alpha_3\beta_3$ δ I II IV-complex (stator). During ATPsynthesis, the proton transport through the enzyme leads to a clockwise movement of the rotor, when viewed from F_0 to F_1, and to synthesis of ATP. During ATP hydrolysis, the sequential binding and hydrolysis of ATP at the three catalytic sites lead to a movement of the rotor in the opposite direction and a concomitant proton translocation through the enzyme. The opposite rotation direction during ATPsynthesis and ATP hydrolysis has been shown recently with single molecule fluorescence spectroscopy [75, 76].

In F_1, subcomplexes that lack subunit δ and subunits I and II, the three αβ-pairs are intrinsically identical. Only the different interactions between γ, ε, and each

αβ-pair give rise to the different conformations. In all X-ray structures reported up to now, this situation is realized. It is essential for the binding change mechanism that all catalytic sites are intrinsically identical; that is, rotation of the central stalk by 120° leads to interactions with the next αβ-pair which are energetically equal to those with the previous αβ-pair. In CF_0F_1 (see Figure 9.1), the situation is different. The presence of subunit δ, and subunits I and II that form the peripheral stalk, gives rise to an asymmetry and, possibly, the binding of I, II, and δ, changes the properties of one α-subunit. If the α-subunit tagged by subunits I and II has a conformation which differs from the two other αβ-pairs, it may have different interactions with the γ-subunit. There are three possibilities for the interaction of the central stalk with the tagged α-subunit: either the central stalk is bound stronger, or weaker, or its binding is unchanged, as compared to the non-tagged α-subunits. Based on this consideration, it is expected to find in an enzyme ensemble one orientation of the central stalk relative to the peripheral stalk in case of stronger interaction, two orientations in case of weaker interaction, and the three orientations in case of identical interaction.

The image reconstruction of vitrified CF_0F_1 shows only one conformation of the enzyme; the homology model of the $\alpha_3\beta_3\gamma\varepsilon$-complex can be fitted optimally only in one position to the central stalk observed in the 3-D map from electron microscopy [32]. This shows that, in the presence of AMPPNP, the H^+-ATP synthase is found in a unique resting position. Notice that, in this state, the conformation of one α-subunit is changed by interaction with the peripheral stalk, leading to an increase in stability of one position of the central stalk within the $\alpha_3\beta_3$-barrel.

Figure 9.5 shows a schematic view of the subunit arrangement looking on to the membrane plane from CF_0 to the CF_1-part. A 0.3 nm slice from the electron density map at CF_0F_1 (grey) is shown, taken from the electron density map at the position marked by a line in Figure 9.4 left. The α-subunits are indicated by magenta circles, the β-subunits by red circles. The α-subunit with the highest density is the one tagged by the peripheral stalk. The model of the central stalks fits optimally only in one position into the αβ-hexagon. In the $\alpha_3\beta_3\gamma$-complex, without the peripheral stalk, the different interactions of the γ-subunit with the αβ-pairs have been used to define the conformations of the different α- and β-subunits (E, D and T) [71]. This nomenclature is adopted for CF_0F_1 and, on this basis, the different conformations can be assigned with respect to the peripheral stalk (see Figure 9.5). The α-subunit tagged by the peripheral stalk has the conformation T.

The activity of CF_0F_1 is strongly regulated by a redox reaction and by a ΔpH dependent activation [77–79]. The redox regulation is due to the redox state of a -S–S-group in the γ subunit which is either in the reduced or oxidized state [80–82]. In the oxidized state, no ATP hydrolysis is observed and, at the same ΔpH, the rate of ATP synthesis is higher in the reduced state than in the oxidized state. The redox regulation seems to be a peculiarity of the photosynthetic H^+-ATP synthases. These enzymes must have a very strict control of activity since they are exposed to both light and dark circles and they have to avoid ATP hydrolysis in the dark period.

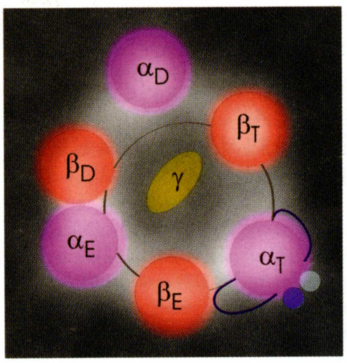

Figure 9.5 Orientation of the peripheral stalk (subunits I and II) and the central stalk (subunit γ) relative to the $\alpha_3\beta_3$-complex in the resting (inactive) state of CF_0F_1. A slice of 0.3 nm thickness from the electron density map of CF_0F_1 as indicated in Figure 9.4 left (line) is shown in a view from CF_0 to the CF_1-part. Magenta circles indicate α-subunits, red circles show β-subunits. Subunits I and II are shown in blue, the γ-subunit is shown in yellow. E, D and T refer to the conformational states of the catalytic nucleotide binding sites. The shape at the III ring is indicated by a brown line and subunit IV is outlined in blue.

Therefore, the redox-state of the H^+-ATP synthase is coupled via ferredoxin and thioredoxin to the redox state of $NADP^+$/NADPH, which changes strongly at light–dark transitions.

CF_0F_1 (in the oxidized and the reduced state) catalyzes neither ATP synthesis nor ATP hydrolysis, when the membrane is not energized. This is expected for the energy requiring ATP synthesis, but it is a surprising observation for energy releasing ATP hydrolysis. Obviously, in the absence of membrane energization, CF_0F_1 is in an inactive state in both redox states. Energization of the membrane by ΔpH or an electric potential difference leads to a conformational change. The enzyme releases a previously tightly bound ADP and it is turned into the metastable active state. Only in this state is the the enzyme able to carry out catalysis [78].

The structure of CF_0F_1 analyzed in the presence of AMPPNP represents the inactive ("resting") state of the enzyme [32]. In the inactive state, there is one preferential position of the central stalk relative to the peripheral stalk. That is, interaction with one of the αβ-pairs leads to a conformational state with the lowest energy. On the other hand, the binding change mechanism proposes a sequence of identical interactions of the central stalk with each of the three αβ-pairs and, consequently, during catalysis, three different orientations of the central stalk, relative to the peripheral stalk, should have the same energy. Based on this consideration, it is concluded that the activation process leads to a structural change between α and the peripheral stalk. In this structure, identical interactions of all three αβ-pairs with the central stalk are possible. Only in this state ("active state") the enzyme is able to catalyze reversibly proton transport coupled ATP synthesis and ATP hydrolysis.

The mechanism of coupling of proton transport with the movement of the III-ring and the γε-complex in combination with the binding change mechanism predicts the number of protons which are translocated through CF_0F_1 per ATP (H^+/ATP ratio). After rotation of the $\gamma\varepsilon III_{14}$ complex by 360° the enzyme has produced 3 ATP (one at each catalytic site) and translocated 14 H^+, that is the H^+/ATP ratio is given by the subunit stoichiometry of subunit III to β.

$$\frac{H^+}{ATP} = \frac{\text{number of III-subunits}}{\text{number of } \beta\text{-subunits}} = \frac{14}{3} = 4.7$$

However, it has been shown for CF_0F_1 that the thermodynamic H^+/ATP ratio is four [83, 84]. This difference may result from the activation. For estimation of H^+/ATP from subunit stoichiometries, it is assumed that at the start and the end of the 360° rotation, the enzyme is in the same state. If the enzyme is in the inactive state before rotation starts, it must be first converted into the metastable active state. Also, this process requires protons, and it might be speculated that 2 protons are necessary for activation of the enzyme and that 12 protons are used for ATP synthesis.

References

1 Mitchell, P. (1961) Coupling of phosphorylation to electron and hydrogen transfer by a chemi-osmotic type of mechanism. *Nature*, **191**, 144–8.

2 Wilkens, S., Borchardt, D., Weber, J. and Senior, A.E. (2005) Structural characterization of the interaction of the delta and alpha subunits of the Escherichia coli F1F0-ATP synthase by NMR spectroscopy. *Biochemistry*, **44**, 11786–94.

3 Wilkens, S., Dunn, S.D., Chandler, J., Dahlquist, F.W. and Capaldi, R.A. (1997) Solution structure of the N-terminal domain of the delta subunit of the E-coli ATPsynthase. *Nature Structural Biology*, **4**, 198–201.

4 Carbajo, R.J., Kellas, F.A., Runswick, M.J., Montgomery, M.G., Walker, J.E. and Neuhaus, D. (2005) Structure of the F1-binding domain of the stator of bovine F1Fo-ATPase and how it binds an alpha-subunit. *Journal of Molecular Biology*, **351**, 824–38.

5 Wilkens, S., Dahlquist, F.W., McIntosh, L.P., Donaldson, L.W. and Capaldi, R.A. (1995) Structural features of the epsilon subunit of the Escherichia coli ATP synthase determined by NMR spectroscopy. *Nature Structural Biology*, **2**, 961–7.

6 Wilkens, S. and Capaldi, R.A. (1998) Solution structure of the epsilon subunit of the F1-ATPase from Escherichia coli and interactions of this subunit with beta subunits in the complex. *The Journal of Biological Chemistry*, **273**, 26645–51.

7 Uhlin, U., Cox, G.B. and Guss, J.M. (1997) Crystal structure of the epsilon subunit of the proton-translocating ATP synthase from Escherichia coli. *Structure*, **5**, 1219–30.

8 Cabezon, E., Runswick, M.J., Leslie, A.G. and Walker, J.E. (2001) The structure of bovine IF1, the regulatory subunit of mitochondrial F-ATPase. *The EMBO Journal*, **20**, 6990–6.

9 Gogol, E.P., Lücken, U., Bork, T. and Capaldi, R.A. (1989) Molecular architecture of Escherichia coli F1 adenosinetriphosphatase. *Biochemistry*, **28**, 4709–16.

10 Gogol, E.P., Aggeler, R., Sagermann, M. and Capaldi, R.A. (1989) Cryoelectron microscopy of Escherichia coli F1 adenosinetriphosphatase decorated with monoclonal antibodies to individual subunits of the complex. *Biochemistry*, **28**, 4717–24.

11 Gogol, E.P., Johnston, E., Aggeler, R. and Capaldi, R.A. (1990) Ligand-dependent structural variations in Escherichia coli F1 ATPase revealed by cryoelectron microscopy. *Proceedings of the National Academy of Sciences of the United States of America*, **87**, 9585–9.

12 Wilkens, S. and Capaldi, R.A. (1994) Asymmetry and structural changes in ECF1 examined by cryoelectronmicroscopy. *Biological Chemistry Hoppe-Seyler*, **375**, 43–51.

13 Boekema, E.J., Van Heel, M. and Gräber, P. (1988) Structure of the ATP synthase from chloroplasts studied by electron-microscopy and image-processing. *Biochimica et Biophysica Acta*, **933**, 365–71.

14 Boekema, E.J., Xiao, J.P. and Mccarty, R.E. (1990) Structure of the ATP synthase from chloroplasts studied by electron-microscopy–localization of the small subunits. *Biochimica et Biophysica Acta*, **1020**, 49–56.

15 Boekema, E.J. and Böttcher, B. (1992) The structure of ATP synthase from chloroplasts–conformational-changes of Cf1 studied by electron-microscopy. *Biochimica et Biophysica Acta*, **1098**, 131–43.

16 Boekema, E.J., Berden, J.A. and van Heel, M.G. (1986) Structure of mitochondrial F1-ATPase studied by electron microscopy and image processing. *Biochimica et Biophysica Acta*, **851**, 353–60.

17 Akey, C.W., Crepeau, R.H., Dunn, S.D., McCarty, R.E. and Edelstein, S.J. (1983) Electron microscopy and single molecule averaging of subunit-deficient F1-ATPases from Escherichia coli and spinach chloroplasts. *The EMBO Journal*, **2**, 1409–15.

18 Tsuprun, V.L., Mesyanzhinova, I.V., Kozlov, I.A. and Orlova, E.V. (1984) Electron microscopy of beef heart mitochondrial F1-ATPase. *FEBS Letters*, **167**, 285–90.

19 Rastogi, V.K. and Girvin, M.E. (1999) Structural changes linked to proton translocation by subunit c of the ATP synthase. *Nature*, **402**, 263–8.

20 Dmitriev, O., Jones, P.C., Jiang, W. and Fillingame, R.H. (1999) Structure of the membrane domain of subunit b of the Escherichia coli F0F1 ATP synthase. *The Journal of Biological Chemistry*, **274**, 15598–604.

21 Del Rizzo, P.A., Bi, Y., Dunn, S.D. and Shilton, B.H. (2002) The "second stalk" of Escherichia coli ATP synthase: structure of the isolated dimerization domain. *Biochemistry*, **41**, 6875–84.

22 Girvin, M.E., Rastogi, V.K., Abildgaard, F., Markley, J.L. and Fillingame, R.H. (1998) Solution structure of the transmembrane H+-transporting subunit c of the F1F0 ATP synthase. *Biochemistry*, **37**, 8817–24.

23 Carbajo, R.J., Silvester, J.A., Runswick, M.J., Walker, J.E. and Neuhaus, D. (2004) Solution structure of subunit F(6) from the peripheral stalk region of ATP synthase from bovine heart mitochondria. *Journal of Molecular Biology*, **342**, 593–603.

24 Takeyasu, K., Omote, H., Nettikadan, S., Tokumasu, F., Iwamoto-Kihara, A. and Futai, M. (1996) Molecular imaging of Escherichia coli F0F1-ATPase in reconstituted membranes using atomic force microscopy. *FEBS Letters*, **392**, 110–13.

25 Singh, S., Turina, P., Bustamante, C.J., Keller, D.J. and Capaldi, R. (1996) Topographical structure of membrane-bound Escherichia coli F1F0 ATP synthase in aqueous buffer. *FEBS Letters*, **397**, 30–4.

26 Birkenhäger, R., Hoppert, M., Deckers-Hebestreit, G., Mayer, F. and Altendorf, K. (1995) The F_0 complex of the Escherichia coli ATP synthase. Investigation by electron spectroscopic imaging and immunoelectron microscopy. *European Journal of Biochemistry*, **230**, 58–67.

27 Böttcher, B., Bertsche, I., Reuter, R. and Gräber, P. (2000) Direct visualization of conformational changes in $EF0F_1$ by electron microscopy. *Journal of Molecular Biology*, **296**, 449–57.

28 Gogol, E.P., Lücken, U. and Capaldi, R.A. (1987) The stalk connecting the F1 and F0 domains of ATP synthase visualized by electron microscopy of unstained specimens. *FEBS Letters*, **219**, 274–8.

29 Wilkens, S. and Capaldi, R.A. (1998) Electron microscopic evidence of two stalks linking the F1 and F0 parts of the Escherichia coli ATP synthase. *Biochimica et Biophysica Acta*, **1365**, 93–7.

30 Neff, D., Tripathi, S., Middendorf, K., Stahlberg, H., Butt, H.J., Bamberg, E. and Dencher, N.A. (1997) Chloroplast F0F1 ATP synthase imaged by atomic force microscopy. *Journal of Structural Biology*, **119**, 139–48.

31 Böttcher, B., Gräber, P., Boekema, E.J. and Lücken, U. (1995) Electron cryomicroscopy of 2-Dimensional crystals of the H^+-ATPase from chloroplasts. *FEBS Letters*, **373**, 262–4.

32 Mellwig, C. and Böttcher, B. (2003) A unique resting position of the ATP-synthase from chloroplasts. *Journal of Biological Chemistry*, **278**, 18544–9.

33 Böttcher, B., Lücken, U. and Gräber, P. (1995) The structure of the H^+-ATPase from chloroplasts by electron cryomicroscopy. *Biochemical Society Transactions*, **23**, 780–5.

34 Böttcher, B., Schwarz, L. and Gräber, P. (1998) Direct indication for the existence of a double stalk in CF0F1. *Journal of Molecular Biology*, **281**, 757–62.

35 Boekema, E.J., Schmidt, G., Gräber, P. and Berden, J.A. (1988) Structure of the Atp-synthase from chloroplasts and mitochondria studied by electron-microscopy. *Zeitschrift fur Naturforschung. C, Journal of Biosciences*, **43**, 219–25.

36 Mellwig, C. and Böttcher, B. (2001) Dealing with particles in different conformational states by electron microscopy and image processing. *Journal of Structural Biology*, **133**, 214–20.

37 Soper, J.W., Decker, G.L. and Pedersen, P.L. (1979) Mitochondrial ATPase complex–dispersed, cytochrome-deficient, oligomycin-sensitive preparation from Rat-Liver containing molecules with a tripartite structural arrangement. *Journal of Biological Chemistry*, **254**, 1170–6.

38 Mörschel, E. and Staehelin, L.A. (1983) Reconstitution of cytochrome-F/B6 and CF_0F_1 ATP synthetase complexes into phospholipid and galactolipid liposomes. *Journal of Cell Biology*, **97**, 301–10.

39 Karrasch, S. and Walker, J.E. (1999) Novel features in the structure of bovine ATP synthase. *Journal of Molecular Biology*, **290**, 379–84.

40 Rubinstein, J.L., Walker, J.E. and Henderson, R. (2003) Structure of the mitochondrial ATP synthase by electron cryomicroscopy. *The EMBO Journal*, **22**, 6182–92.

41 Groth, G. and Pohl, E. (2001) The structure of the chloroplast F1-ATPase at 3.2 Å resolution. *The Journal of Biological Chemistry*, **276**, 1345–52.

42 Groth, G. (2002) Structure of spinach chloroplast F1-ATPase complexed with the phytopathogenic inhibitor tentoxin. *Proceedings of the National Academy of Sciences of the United States of America*, **99**, 3464–8.

43 Hausrath, A.C., Gruber, G., Matthews, B.W. and Capaldi, R.A. (1999) Structural features of the gamma subunit of the Escherichia coli F_1 ATPase revealed by a 4.4-A resolution map obtained by x-ray crystallography. *Proceedings of the National Academy of Sciences of the United States of America*, **96**, 13697–702.

44 Kabaleeswaran, V., Puri, N., Walker, J.E., Leslie, A.G. and Mueller, D.M. (2006) Novel features of the rotary catalytic mechanism revealed in the structure of yeast F1 ATPase. *The EMBO Journal*, **25**, 5433–42.

45 Gibbons, C., Montgomery, M.G., Leslie, A.G. and Walker, J.E. (2000) The structure of the central stalk in bovine F_1 ATPase at 2.4 A resolution. *Nature Structural Biology*, **7**, 1055–61.

46 Rodgers, A.J. and Wilce, M.C. (2000) Structure of the gamma-epsilon complex of ATP synthase. *Nature Structural Biology*, **7**, 1051–4.

47 Hausrath, A.C., Capaldi, R.A. and Matthews, B.W. (2001) The conformation of the epsilon- and gamma-subunits within the Escherichia coli F_1 ATPase. *The Journal of Biological Chemistry*, **276**, 47227–32.

48 Cabezon, E., Montgomery, M.G., Leslie, A.G. and Walker, J.E. (2003) The structure of bovine F1-ATPase in complex with its regulatory protein IF1. *Nature Structural Biology*, **10**, 744–50.

49 Cabezon, E., Arechaga, I., Jonathan, P., Butler, G. and Walker, J.E. (2000) Dimerization of bovine F1-ATPase by binding the inhibitor protein, IF1. *The Journal of Biological Chemistry*, **275**, 28353–5.

50 Stock, D., Leslie, A.G. and Walker, J.E. (1999) Molecular architecture of the rotary motor in ATP synthase. *Science*, **286**, 1700–5.

51 Meier, T., Polzer, P., Diederichs, K., Welte, W. and Dimroth, P. (2005) Structure of the rotor ring of F-Type Na^+-ATPase from Ilyobacter tartaricus. *Science*, **308**, 659–62.

52 Stahlberg, H., Müller, D.J., Suda, K., Fotiadis, D., Engel, A., Meier, T., Matthey, U. and Dimroth, P. (2001) Bacterial Na^+-ATP synthase has an undecameric rotor. *EMBO Reports*, **2**, 229–33.

53 Seelert, H., Poetsch, A., Dencher, N.A., Engel, A., Stahlberg, H. and Müller, D.J. (2000) Proton-powered turbine of a plant motor. *Nature*, **405**, 418–19.

54 Müller, D.J., Dencher, N.A., Meier, T., Dimroth, P., Suda, K., Stahlberg, H., Engel, A., Seelert, H. and Matthey, U. (2001) ATP synthase: constrained stoichiometry of the transmembrane rotor. *FEBS Letters*, **504**, 219–22.

55 Fromme, P., Boekema, E.J. and Gräber, P. (1987) Isolation and characterization of a supramolecular complex of subunit-Iii of the ATP synthase from chloroplasts. *Zeitschrift fur Naturforschung. C, Journal of Biosciences*, **42**, 1239–45.

56 Seelert, H., Dencher, N.A. and Müller, D.J. (2003) Fourteen protomers compose the oligomer III of the proton-rotor in spinach chloroplast ATP synthase. *Journal of Molecular Biology*, **333**, 337–44.

57 Dickson, V.K., Silvester, J.A., Fearnley, I.M., Leslie, A.G. and Walker, J.E. (2006) On the structure of the stator of the mitochondrial ATP synthase. *The EMBO Journal*, **25**, 2911–18.

58 Nelson, N., Nelson, H. and Racker, E. (1972) Partial resolution of the enzymes catalyzing photophosphorylation. XII. Purification and properties of an inhibitor isolated from chloroplast coupling factor 1. *The Journal of Biological Chemistry*, **247**, 7657–62.

59 Moroney, J.V., Lopresti, L., McEwen, B.F., McCarty, R.E. and Hammes, G.G. (1983) The Mr-value of chloroplast coupling factor 1. *FEBS Letters*, **158**, 58–62.

60 Süss, K.-H. and Schmidt, O. (1982) Evidence for an α_3, β_3, γ, δ, I, II, ε, III_5 subunit stoichiometry of chloroplast ATP synthetase complex (CF_1-CF_0). *FEBS Letters*, **144**, 213–18.

61 Fromme, P., Gräber, P. and Salnikow, J. (1987) Isolation and identification of a 4th subunit in the membrane part of the chloroplast ATP-Synthase. *FEBS Letters*, **218**, 27–30.

62 Pick, U. and Racker, E. (1979) Purification and reconstitution of the N,N'-dicyclohexylcarbodiimide-sensitive ATPase complex from spinach chloroplasts. *The Journal of Biological Chemistry*, **254**, 2793–9.

63 Steigmiller, S., Börsch, M., Gräber, P. and Huber, M. (2005) Distances between the b-subunits in the tether domain of F0F1-ATP synthase from E. coli. *Biochimica et Biophysica Acta*, **1708**, 143–53.

64 Boyer, P.D. (1993) The binding change mechanism for ATP synthase–some probabilities and possibilities. *Biochimica et Biophysica Acta*, **1140**, 215–50.

65 Wilkens, S., Zhou, J., Nakayama, R., Dunn, S.D. and Capaldi, R.A. (2000) Localization of the delta subunit in the Escherichia coli F(1)F(0)-ATPsynthase by immuno electron microscopy: the delta subunit binds on top of the F(1). *Journal of Molecular Biology*, **295**, 387–91.

66 Boyer, P.D. (1998) ATP synthase–past and future. *Biochimica et Biophysica Acta*, **1365**, 3–9.

67 Junge, W. (2004) Protons, proteins and ATP. *Photosynthesis Research*, **80**, 197–221.

68 Junge, W., Lill, H. and Engelbrecht, S. (1997) ATP synthase: an electrochemical transducer with rotatory mechanics. *Trends in Biochemical Sciences*, **22**, 420–3.

69 Marti-Renom, M.A., Stuart, A.C., Fiser, A., Sanchez, R., Melo, F. and Sali, A. (2000)

Comparative protein structure modeling of genes and genomes. *Annual Review of Biophysics and Biomolecular Structure*, **29**, 291–325.

70 Finn, R.D., Mistry, J., Schuster-Bockler, B., Griffiths-Jones, S., Hollich, V., Lassmann, T., Moxon, S., Marshall, M., Khanna, A., Durbin, R., Eddy, S.R., Sonnhammer, E.L. and Bateman, A. (2006) Pfam: clans, web tools and services. *Nucleic Acids Research*, **34**, D247–51.

71 Abrahams, J.P., Leslie, A.G.W., Lutter, R. and Walker, J.E. (1994) Structure at 2.8-angstrom resolution of F1-Atpase from bovine heart-mitochondria. *Nature*, **370**, 621–8.

72 McLachlin, D.T., Coveny, A.M., Clark, S.M. and Dunn, S.D. (2000) Site-directed cross-linking of b to the alpha, beta, and a subunits of the Escherichia coli ATP synthase. *The Journal of Biological Chemistry*, **275**, 17571–7.

73 Meier, T., Matthey, U., Henzen, F., Dimroth, P. and Müller, D.J. (2001) The central plug in the reconstituted undecameric c cylinder of a bacterial ATP synthase consists of phospholipids. *FEBS Letters*, **505**, 353–6.

74 Eisfeld, J. (2003) *Physikalische Chemie II*, University of Freiburg, Freiburg.

75 Diez, M., Zimmermann, B., Borsch, M., Konig, M., Schweinberger, E., Steigmiller, S., Reuter, R., Felekyan, S., Kudryavtsev, V., Seidel, C.A. and Graber, P. (2004) Proton-powered subunit rotation in single membrane-bound F0F1-ATP synthase. *Nature Structural and Molecular Biology*, **11**, 135–41.

76 Zimmermann, B., Diez, M., Zarrabi, N., Graber, P. and Borsch, M. (2005) Movements of the epsilon-subunit during catalysis and activation in single membrane-bound H(+)-ATP synthase. *The EMBO Journal*, **24**, 2053–63.

77 Kramer, D.M., Wise, R.R., Frederick, J.R., Alm, D.M., Hesketh, J.D., Ort, D.R. and Crofts, A.R. (1990) Regulation of coupling factor in field-grown sunflower–a redox model relating coupling factor activity to the activities of other thioredoxin-dependent chloroplast enzymes. *Photosynthesis Research*, **26**, 213–22.

78 Gräber, P., Schlodder, E. and Witt, H.T. (1977) Conformational change of the chloroplast ATPase induced by a transmembrane electric field and its correlation to phosphorylation. *Biochimica et Biophysica Acta*, **461**, 426–40.

79 Junesch, U. and Gräber, P. (1987) Influence of the redox state and the activation of the chloroplast ATP-synthase on proton-transport coupled ATP-synthesis/hydrolysis. *Biochimica et Biophysica Acta*, **893**, 275–88.

80 Nalin, C.M. and McCarty, R.E. (1984) Role of a disulfide bond in the gamma subunit in activation of the ATPase of chloroplast coupling factor 1. *The Journal of Biological Chemistry*, **259**, 7275–80.

81 Groth, G. and Strotmann, H. (1999) *Physiologia Plantarum*, **106**, 142–8.

82 Richter, M.L., Samra, H.S., He, F., Giessel, A.J. and Kuczera, K.K. (2005) Coupling proton movement to ATP synthesis in the chloroplast ATP synthase. *Journal of Bioenergetics and Biomembranes*, **37**, 467–73.

83 Van Walraven, H.S., Strotmann, H., Schwarz, O. and Rumberg, B. (1996) The H+/ATP coupling ratio of the ATP synthase from thiol-modulated chloroplasts and two cyanobacterial strains is four. *FEBS Letters*, **379**, 309–13.

84 Turina, P., Samoray, D. and Gräber, P. (2003) H^+/ATP ratio of proton transport-coupled ATP synthesis and hydrolysis catalysed by $CF0F_1$-liposomes. *The EMBO Journal*, **22**, 418–26.